



## Regular article

P-InAsSbP/p-InAs<sub>0.88</sub>Sb<sub>0.12</sub>/n-InAs<sub>0.88</sub>Sb<sub>0.12</sub>/n<sup>+</sup>-InAs PDs with a smooth p-n junctionN.D. Il'inskaya<sup>a</sup>, S.A. Karandashev<sup>a</sup>, A.A. Lavrov<sup>a,b</sup>, B.A. Matveev<sup>a</sup>, M.A. Remennyi<sup>a,\*</sup>, N.M. Stus'<sup>a</sup>, A.A. Usikova<sup>a</sup><sup>a</sup> Ioffe Institute, 26 Politekhnicheskaya, St. Petersburg 194021, Russian Federation<sup>b</sup> IoffeLED, Ltd., 26 Politekhnicheskaya, St. Petersburg 194021, Russian Federation

## HIGHLIGHTS

- Linear impurity distribution near the p-n junction.
- Low unit area capacity ( $C_0/A$ )<sub>77K</sub> =  $4.3 \times 10^{-8} \text{ F} \times \text{cm}^{-2}$ ).
- $D_{4.7\mu\text{m},300\text{K}}^*$  as high as  $6.5 \times 10^8$  Jones.

## ARTICLE INFO

## Article history:

Received 20 September 2017

Revised 2 November 2017

Accepted 3 November 2017

Available online 4 November 2017

© 2017 Elsevier B.V. All rights reserved.

## Annotation

Current-voltage, capacitance-voltage, and photoelectrical characteristics of *InAs*<sub>0.88</sub>*Sb*<sub>0.12</sub> photodiodes grown onto *InAs* substrates with a smooth p-n junction and various mesa diameters and layer thicknesses sensitive to radiation with wavelengths up to 5.5 μm were investigated and analyzed. Conclusions on the impact of the *InAs*<sub>0.88</sub>*Sb*<sub>0.12</sub>-layer thickness on the main performance parameters (zero bias resistance, sensitivity, and spectral response) are presented and discussed.

## 1. Introduction

There has been growing interest in the *InAsSb* ternary alloy as a material for the “bulk” absorbing layer in unipolar (or “barrier”) [1–4] and bipolar [5–12] detectors operating in the mid-IR spectral range including those with wide-gap “barrier” layers and a p-n junction [5,7,9–11]. The applications for these detectors are in optical gas detection [13] and radiometric temperature measurements [14] as well as in thermal imaging.

One of the basic advantages of *InAsSb*-based photodiodes (PDs) and barrier detectors over other types of detectors, e.g., pyroelectric

ones, is their short response time. These response times are a key feature of large area focal plane detector arrays. The conventional method to decrease the PD response time is by creating a smooth/linear impurity distribution that enables enhancement of the space charge region width. It is common to anticipate that utilizing a thick space charge region leads to a reduced PD capacitance (*C*) with respect to PDs with an abrupt p-n junction. Correspondingly, the resistance-capacitance product (*RC*)/response time ( $\tau_{RC}$ ) as well as the tunnel currents in smooth p-n junctions are expected to be low. However, to the best of our knowledge, there have not been many attempts to create p-i-n *InAsSb* diodes, with only a few papers mentioned in article overviews (see, e.g., [15]). There is also very little data on the C-V characteristics of *InAsSb* “bulk” detectors: the capacitance data is limited to numbers at low temperatures [16,17] with no data mentioned in the overviews (see, e.g., [15]). Moreover, the spectral response in many of the *InAsSb*-based detectors with barrier layers suffers from sensitivity degradation in the low photon energy region where  $h\nu$  approaches  $E_g$  [5,9,10].

In this paper, we present the experimental results for back-side illuminated (BSI) P-*InAsSbP*(*Zn*)/p-*InAsSb*<sub>0.12</sub>(*Zn*)/n-*InAsSb*<sub>0.12</sub>/n<sup>+</sup>-*InAs*(*Sn*) double heterostructure (DH) PDs operating at near room temperature and having *InAs*<sub>0.88</sub>*Sb*<sub>0.12</sub> absorbers of different thicknesses and smooth *Zn* distribution in the vicinity of the p-n junction.

\* Corresponding author.

E-mail address: [mremennyi@mail.ioffe.ru](mailto:mremennyi@mail.ioffe.ru) (M.A. Remennyi).

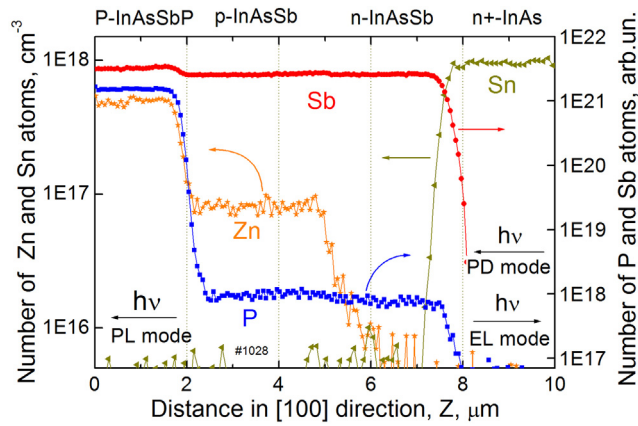


**Fig. 1.** Distribution of *P*, *Zn*, *Sn*, and *Sb* atoms along the growth direction (SIMS data). Arrows on the right and left denote photon flux with respect to the heterostructure layers at the PL, PD, and EL measurement modes.

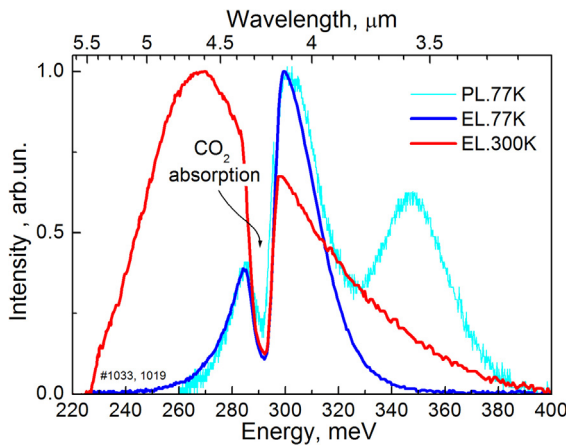


**Fig. 2.** Photoluminescence (PL) and electroluminescence (EL) spectra of typical *InAsSb*<sub>0.12</sub>-based PDs (see arrows in Fig. 1 that clarify the measurement conditions).

## 2. Experimental details

DH samples were grown by the LPE method at  $\sim 650^\circ\text{C}$  onto heavily doped  $n^+$ -*InAs(Sn)* substrates (100) ( $n^+ = 1 \times 10^{18} \text{ cm}^{-3}$ ) that were transparent in the 3–6  $\mu\text{m}$  spectral range. The samples differed slightly from those reported earlier in [8] as *InSb* mole fraction was higher in the ternary alloys and DH additionally contained a 2–3  $\mu\text{m}$  thick *p-InAs*<sub>0.88</sub>*Sb*<sub>0.12</sub> (*Zn*) layer placed between an undoped *n-InAs*<sub>0.88</sub>*Sb*<sub>0.12</sub> layer and a wide gap quaternary *P-InAs*<sub>1-x-y</sub>*Sb*<sub>x</sub>*P*<sub>y</sub>(*Zn*) cladding (or contact/top layer). The *n-InAsSb*-layer thickness in the different structures varied from 3 up to 15  $\mu\text{m}$ , while the *P-InAsSbP* claddings in all samples were 2–3  $\mu\text{m}$  thick.

Secondary ion mass spectrometry (SIMS) measurements revealed abrupt changes in the *P*, *Sb*, and *Sn* concentrations at the heterojunctions and a smooth distribution of *Zn* atoms along the growth direction as shown in Fig. 1. In accordance with the data in Fig. 1 (see, e.g., the data points between  $z = 5 \mu\text{m}$  and  $z = 8 \mu\text{m}$ ), there is a drop in the *Zn* concentration by about 10 volume units at a distance of about 1  $\mu\text{m}$  that takes place.

Photo- (PL) and electroluminescence (EL) spectra measured in reflection and transmission geometry modes (see Fig. 2) were fairly close to those reported previously in [8] with minor deviations in the peak energy values  $h\nu_{\text{max}}$  from the old data. In accordance with Fig. 2 they amounted to  $h\nu_{\text{max}}^{\text{EL,300K}} = 270 \text{ meV}$  for EL coming from *InAsSb* at room temperature (RT),  $h\nu_{\text{max}}^{\text{77K}} = 310 \text{ meV}$  for both EL

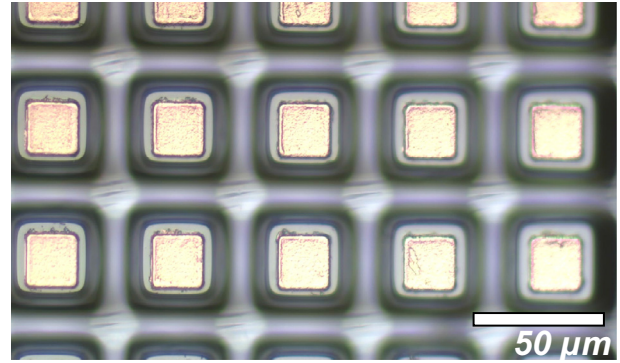


**Fig. 3.** Photo of the epi-side/contact side of the  $8 \times 64$  PD array.

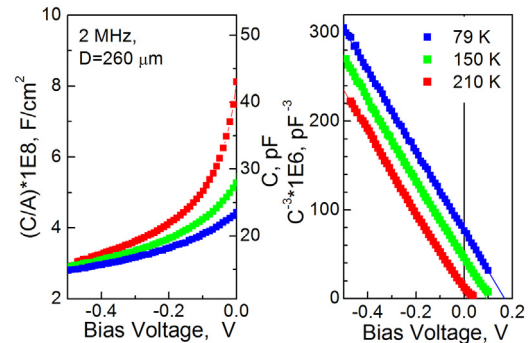


**Fig. 4.** C-V characteristics in *InAsSb*<sub>0.12</sub> PDs at 79, 150, and 210 K.

and PL coming from *InAsSb*, and  $h\nu_{\text{max}}^{\text{PL,77K}} = 356 \text{ meV}$  for PL coming from *InAsSbP* at 77 K. The RT EL peak was close enough to the responsivity peak ( $h\nu_{\text{max}}^{\text{PD}} = 264 \text{ meV}$ ) for most of the investigated PDs.

Standard optical photolithography and wet chemical etching processes were implemented to obtain chips of a ( $8 \times 64$ ) matrix and single element PDs with 35–260  $\mu\text{m}$  wide square or circular mesas capable of working in BSI mode. The single element chip design was the same as in [18]; the  $8 \times 64$  monolithic array contained 10  $\mu\text{m}$  high and 35  $\mu\text{m}$  wide square mesas/elements “printed” with a period of 50  $\mu\text{m}$  (see Fig. 3).

Broad Ohmic contacts were formed by evaporation of *Ag(Mn)-Ni-Au* and *Cr-Au-Ni-Au* metal compositions at vacuum for the anodes and cathodes, respectively. Previous measurements with metal and semiconductor compositions similar to the above revealed that both contacts were reflective [18]. In small area PDs, the anode covered about 0.56 of the mesa area (see Fig. 3) while in large area PDs, the above number was as high as 0.9. No attempts were undertaken to passivate the mesa side walls or to create an antireflection coating onto the  $n^+$ -*InAs* outcoupling surface.

IR images at  $\lambda = 3 \mu\text{m}$  consisting of  $128 \times 128$  pixels were obtained using methods and equipment reported previously in [18,19]; current-voltage (I-V), capacitance-voltage (C-V), and spectral characteristics were measured using the same setups as in [8].

## 3. Results and discussion

The nearly linear dependence of  $(C)^{-3}$  on bias voltage in the temperature range of 79–210 K (see Fig. 4) indicates a linear impurity distribution near the p-n junction that goes along with the smooth spatial distribution of *Zn* atoms presented in Fig. 1 and this

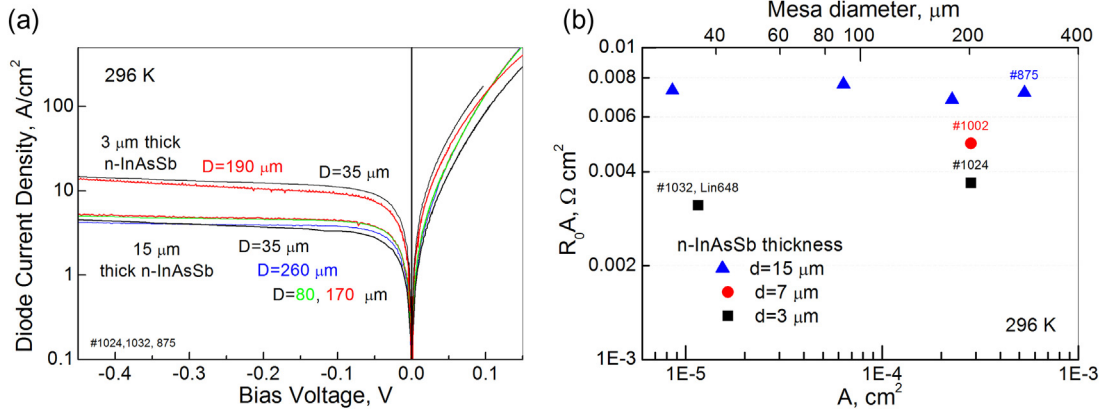


Fig. 5. (a) RT I-V characteristics of PDs with different lateral sizes and n-InAsSb<sub>0.12</sub>-layer thickness and, (b) dependence of the zero bias resistance area product on area at RT.

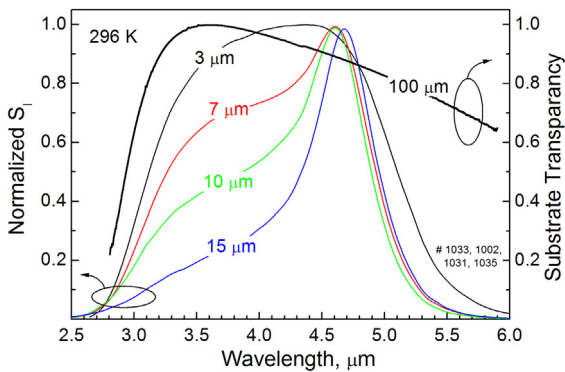


Fig. 6. Relative spectral response of PDs with different InAsSb<sub>0.12</sub>-layer thicknesses and 0.1 mm thick n<sup>+</sup>-InAs transparency spectrum at RT.

distinguished the current samples from many published ones, that is, from those with an abrupt p-n junction (see e.g., [16]). The unit area capacitance at zero bias ( $C_0/A$ ) at 77 K amounted to  $4.3 \times 10^{-8} \text{ F} \times \text{cm}^{-2}$  which is somewhat less than in our previous samples in [16] and is about 3 times smaller than that for the nearest analog - InAsSbP/InAs single heterostructure PDs with a smooth p-n junction in [20]. A feature in common with PDs in [20] was also an independence of the slope in the  $(C)^{-3} - (V)$  coordinates on temperature. This feature is typical for semiconductors with low concentration of the electrically active deep centers. At 210 K the  $RC_0$  product for a standard load of  $50 \Omega$  was about 2.2 ns for a 260 μm wide PD.

Fig. 5 shows RT dark current I-V characteristics for a set of PDs with different mesa diameters and different n-InAsSb-layer thicknesses. As seen from Fig. 5a, the diode current in PDs with a thick InAsSb layer scales well with the mesa area and thus a negligible dependence of zero bias resistance area product ( $R_0A$ ) on the PD active area dimensions is taking place (see Fig. 5b). PDs with thin InAsSb layers exhibit smaller  $R_0A$  values with respect to their thick analogs and a decrease of the  $R_0A$  value in small area PDs.

Our understanding is that small  $R_0A$  value in the described InAsSb/InAs PDs with respect to other PDs originates mostly from low energy gap value rather than from large lattice mismatch. The statement goes along with the dependence of  $R_0A$  on red cut-off energy  $h\nu_{0.1}$  in a set of InAsSb PD analogs with different lattice mismatch values presented in [21] where  $R_0A \sim \exp(-h\nu_{0.1}/kT)$  for  $h\nu_{0.1} = 150\text{--}410 \text{ meV}$ .

The forward bias I-V characteristics followed the modified Shockley formula ( $J_{\text{dark}} = J_0(\exp(eV/\beta kT) - 1)$  with the ideality factor ( $\beta$ ) being nearly unity for thick and 1.3 for thin PDs indicating a contribution of generation-recombination current and/or the

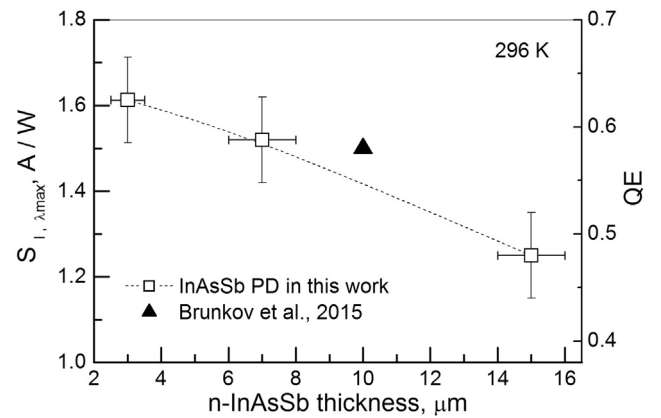
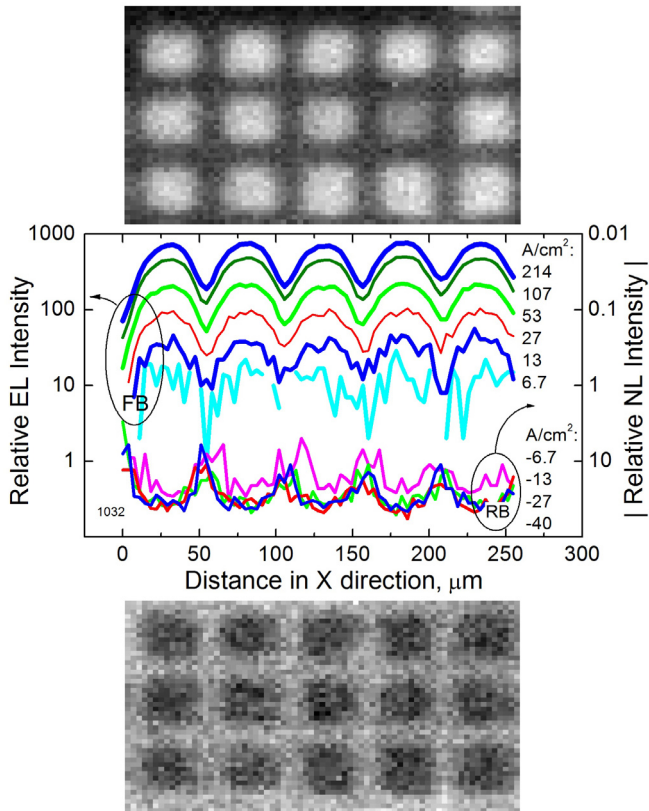


Fig. 7. PD current sensitivity (left scale) and QE (right scale) at maximum vs. the n-InAsSb<sub>0.12</sub>-layer thickness at RT.

presence of some kind of leakage in the latter case. Both relatively low  $R_0A$  and elevated  $\beta$  values in thin PDs at RT correlate with previous observations of the  $D^*$  value enhancement as the InAsSb buffer layer thickness increases [7]. The RT dark current  $J_{\text{dark}}^{300K}$  in small area PDs appeared comparable with several instances of previously published data for the MBE grown detectors, e.g., our thin PDs at  $-0.3 \text{ V}$  exhibit nearly the same current density values  $J_{\text{dark}}^{300K}$  as the InAsSb<sub>0.13</sub> p-i-n diodes at  $-0.1 \text{ V}$ , while the  $J_{\text{dark}}^{300K}$  in thick PDs at  $-0.5 \text{ V}$  is fairly close to the numbers for the 200 μm wide AlGaAsSb / InAsSb<sub>0.21</sub> n-B-n detector at  $-0.5 \text{ V}$  in [4].

The RT responsivity for shortwaves was progressively enhanced as the PD active layer thickness was decreased as shown in Fig. 6. The shortwave shoulder of the thin PDs relates to the n<sup>+</sup>-InAs transparency spectrum slope, while the longwave shoulders were nearly independent of the InAsSb-layer thickness. The responsivity at wavelengths far enough from both cut-offs was nearly exponentially dependent on the n-InAsSb-layer thickness reflecting diffusion limited collection of carriers. Draft estimation of the hole diffusion length was  $L_p^{RT} = 5\text{--}7.5 \mu\text{m}$ ; these numbers are close to estimations of the same parameter given in [2,11] and about two times larger than in [4] for the n-InAs<sub>0.9</sub>Sb<sub>0.1</sub>-based PDs.

Fig. 7 presents the sensitivity at maximum vs. the n-InAsSb-layer thickness; as seen from Fig. 7, the 3-μm thick layer is still absorbing sufficient amounts of the incoming radiation at the peak wavelength so that the sensitivity is enhanced due to the smaller distance to the p-n junction and coherently better charge carrier collection. The RT sensitivity value for the 3-μm thick



**Fig. 8.** EL (at the top), NL (at the bottom) images and distribution of EL and NL intensity in the activated PD array.

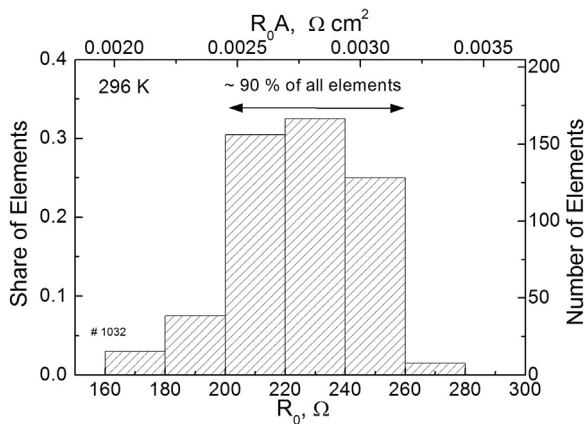


**Fig. 9.** Histogram of the distribution of zero bias resistance in an  $8 \times 64$  *InAsSb* PD array.

*InAsSb*-layer PD is about two times higher than that for most barrier detectors with the same absorbing layer composition [9,10] and several times of that presented in [12] for the DH PD. At RT, the  $D_{4.7\mu\text{m},300\text{K}}^*$  was as high as  $6.5 \times 10^8$  Jones.

Fig. 8 presents IR images of the 15 activated elements of the  $8 \times 64$  PD array at forward/EL and reverse/negative luminescence (NL) bias/mode with corresponding distribution of the radiation intensity along the “horizontal” direction at several currents shown in the center of Fig. 8. The mesa walls were inclined with respect to the incoming/outcoming radiation and thus both the NL and EL images provide no strong contrast, that is, no plateaus in NL and EL spatial distribution. The NL intensity was already saturated at

a current density of about  $13 \text{ A/cm}^2$ ; previously, nearly the same value for the saturation current  $J_0$  were measured in close structures but with much larger mesa dimensions [8]. The  $J_{\text{dark}}^{300\text{K}}$  value at  $-0.1 \text{ V}$  for the array element was somewhat smaller than in single element *InAsSb*<sub>0.13</sub> p-i-n PDs [4].

Good array uniformity (in addition to the data in Fig. 8) is also demonstrated by a histogram of zero bias resistance distribution in an unassembled chip shown in Fig. 9. As seen from the histogram, about 90% of all elements had the  $R_0A$  value in the  $0.0025\text{--}0.0032 \text{ } \Omega \times \text{cm}^2$  range. This value is fairly close to those for the single element *InAsSb* PDs mentioned in [8] and to data in Fig. 5. Normally, the individual PDs exhibit much better  $R_0A$  values than their matrix “clones” [15] and thus we consider the above coincidence to be a remarkable step towards creation of high performance mid-IR FPA.

#### 4. Conclusion

*P-InAsSbP(Zn)/p-InAs<sub>0.88</sub>Sb<sub>0.12</sub>/n-InAs<sub>0.88</sub>Sb<sub>0.12</sub>/n<sup>+</sup>-InAs* single element and matrix ( $8 \times 64$ ) heterostructure PDs with a smooth p-n junction and cut-off at  $\lambda_{0.1}^{300\text{K}} = 5.5 \text{ } \mu\text{m}$  with domination of the diffusion current and various *n-InAs<sub>0.88</sub>Sb<sub>0.12</sub>*-layer thicknesses were fabricated and studied. A decrease in the absorbing *InAs<sub>0.88</sub>Sb<sub>0.12</sub>*-layer thickness (from 15 down to  $3 \text{ } \mu\text{m}$ ) resulted in a current sensitivity enhancement (from 1.2 up to  $1.6 \text{ A/W}$ ) as well as an increase in the sensitivity spectra full width at half maximum FWHM (from  $0.5$  up to  $2.1 \text{ } \mu\text{m}$ ) due to better collection of photo-generated carriers at room temperature. Unfortunately this enhancement was accompanied/balanced by a twofold  $R_0A$  degradation (from  $0.07$  down to  $0.03 \text{ } \Omega \times \text{cm}^2$ ) making the  $D^*$  value nearly “stable” against *InAsSb*-layer thickness variations. Reasonably high detectivity values ( $D_{4.7\mu\text{m},300\text{K}}^* = 6.5 \times 10^8$  Jones) together with low unit area capacity ( $C_0/A_{77\text{K}} = 4.3 \times 10^{-8} \text{ F} \times \text{cm}^{-2}$ ) promises future fabrication of efficient mid-IR matrix *InAs<sub>0.88</sub>Sb<sub>0.12</sub>*-based PDs operating at room temperature with short response times.

#### Acknowledgments

We would like to thank A.S. Petrov (Open Society, Central Research Institute, “Electron”) for helpful discussions and also A. L. Zakgeim and A.V. Chernyakov who were responsible for successful measurements of near-field EL and NL intensity distribution performed at the Center of Multi-User Facilities, “Element Base of Microwave Photonics and Nanoelectronics: Technology, Diagnostics, Metrology”. The SIMS measurements were carried out at the Center of Shared Scientific Equipment, “Material Science and Diagnostics for Advanced Technologies” (Ioffe Institute). The work performed at IoffeLED, Ltd. was supported by the RF state program, Development of Fabrication Processes for Semiconductor Materials for Use in Matrix Photodetectors and Thermal Vision, Contract No. 14.576.21.0057, ID: RFMEFI57614X0057.

#### Conflict of interest

There is no conflict of interest.

#### References

- [1] P. Klipstein, O. Klin, S. Grossman, N. Snapi, I. Lukomsky, M. Brumer, M. Yassen, D. Aronov, E. Berkowicz, A. Glzman, T. Fishman, O. Magen, I. Shtrichman, E. Weiss, MWIR *InAsSb* XBnn detector (bariodes) arrays operating at 150 K, in: B.F. Andresen, G.F. Fulop, P.R. Norton (Eds.), *Infrared Technology and Applications XXXVII*, Proc. of SPIE Vol. 8012 80122R-1-9, <<https://doi.org/10.1117/12.883238>>.
- [2] A. Soibel, C.J. Hill, S.A. Keo, L. Hoglund, R. Rosenberg, R. Kowalczyk, A. Khoshakhlagh, A. Fisher, D.Z.Y. Ting, S.D. Gunapala, Room temperature

- performance of mid-wavelength infrared InAsSb nBn detectors, *Appl. Phys. Lett.* 105 (2014) 023512, <https://doi.org/10.1063/1.4890465>.
- [3] N. Baril, A. Brown, P. Maloney, M. Tidrow, D. Lubyshev, Y. Qui, J.M. Fastenau, A. W.K. Liu, S. Bandara, Bulk InAs<sub>x</sub>Sb<sub>1-x</sub> nBn photodetectors with greater than 5 μm cutoff on GaSb, *Appl. Phys. Lett.* 109 (2016) 122104, <https://doi.org/10.1063/1.4963069>.
- [4] A.P. Craig, A.R.J. Marshall, Z.-B. Tian, S. Krishna, A. Krier, Mid-infrared InAs<sub>0.79</sub>Sb<sub>0.21</sub>-based nBn photodetectors with Al<sub>0.9</sub>Ga<sub>0.2</sub>As<sub>0.1</sub>Sb<sub>0.9</sub> barrier layers, and comparisons with InAs<sub>0.87</sub>Sb<sub>0.13</sub> p-i-n diodes, both grown on GaAs using interfacial misfit arrays, *Appl. Phys. Lett.* 103 (2013) 253502, <https://doi.org/10.1063/1.4844615>.
- [5] D. Wang, D. Donetsky, G. Kipshidze, Y. Lin, L. Shterengas, G. Belenky, W. Sarney, S. Svensson, Metamorphic InAsSb-based barrier photodetectors for the long wave infrared region, *Appl. Phys. Lett.* 103 (2013) 051120, <https://doi.org/10.1063/1.4817823>.
- [6] K. Mohammed, F. Capasso, R.A. Logan, J.P. van der Ziel, A.L. Hutchinson, High-Detectivity InAs<sub>0.85</sub>Sb<sub>0.15</sub>/InAs Infrared (1.8–4.8 μm) Detectors, *Electron. Lett.* 22 (1986) 215–216.
- [7] A. Krier, W. Suleiman, Uncooled photodetectors for the 3–5 μm spectral range based on III–V heterojunctions, *Appl. Phys. Lett.* 89 (2006) 083512.
- [8] P.N. Brunkov, N.D. Il'inskaya, S.A. Karandashev, A.A. Lavrov, B.A. Matveev, M.A. Remennyi, N.M. Stus', A.A. Usikova, InAsSbP/InAs<sub>0.9</sub>Sb<sub>0.1</sub>/InAs DH photodiodes (λ<sub>0.1</sub> = 5.2 μm, 300 K) operating in the 77–353 K temperature range, *Infrared Phys. Technol.* 73 (2015) 232–237.
- [9] A. Rakovska, V. Berger, X. Marcadet, B. Vinter, G. Glastre, T. Oksenhendler, D. Kaplan, Room temperature InAsSb photovoltaic midinfrared detector, *Appl. Phys. Lett.* 77 (3) (2000) 397–399.
- [10] H. Ait-Kaci, J. Nieto, J.B. Rodriguez, P. Grech, F. Chevrier, A. Salesses, A. Joullié, P. Christol, Optimization of InAsSb photodetector for non-cryogenic operation in the mid-infrared range, *Phys. Stat. Sol. (a)* 202 (4) (2005) 647–651, <https://doi.org/10.1002/pssa.200460456>.
- [11] G. Marre, B. Vinter, V. Berger, Strategy for the design of a non-cryogenic quantum infrared detector, *Semicond. Sci. Technol.* 18 (2003) 284–291, PII: S0268-1242(03)40168-5.
- [12] P. Chakrabarti, A. Krier, A.F. Morgan, Double-heterojunction photodetector for midinfrared applications: theoretical model and experimental results, *Opt. Eng.* 42 (9) (September 2003) 2614–2623.
- [13] J. Hodgkinson, R.P. Tatam, Optical gas sensing: a review, *Meas. Sci. Technol.* 24 (2013) 012004.
- [14] D. Zymelka, B. Matveev, S. Aleksandrov, G. Sotnikova, G. Gavrilov, M. Saadaoui, Time resolved study of variable frequency microwave processing of silver nanoparticles printed onto plastic substrates, *IOP J. Flexible and Printed Electronics* 2 (2017) 045006, <https://doi.org/10.1088/2058-8585/aa900a>.
- [15] A. Rogalski, *Infrared Detectors*, 2-nd edition, International Standard Book Number: 978-1-4200-7671-4, CRC press, Taylor and Francis group, 2012.
- [16] B.A. Matveev, M.P. Mikhailova, N.N. Smirnova, N.M. Stus', G.N. Talalakin, Avalanche multiplication in p-n junctions in InAsSb, *Sov. Phys. Semicond.* 13 (3) (1979) 294–297.
- [17] N.D. Il'inskaya, S.A. Karandashev, N.G. Karpukhina, A.A. Lavrov, B.A. Matveev, M.A. Remennyi, N.M. Stus', A.A. Usikova, Photodiode 1 × 64 Linear Array Based on a Double p-InAsSbP/n-InAs<sub>0.92</sub>Sb<sub>0.08</sub>/n+-InAs Heterostructure, *Semiconductors* 50 (5) (2016) 646–651, <https://doi.org/10.1134/S1063782616050122>.
- [18] A.L. Zakgeim, N.D. Il'inskaya, S.A. Karandashev, A.A. Lavrov, B.A. Matveev, M.A. Remennyi, N.M. Stus', A.A. Usikova, A.E. Cherniakov, Spatial redistribution of radiation in flip-chip photodiodes based on InAsSbP/InAs double heterostructures, *Semiconductors* 51 (2) (2017) 260–266, <https://doi.org/10.1134/S1063782617020269>.
- [19] V.M. Bazovkin, A.A. Guzev, A.P. Kovchavtsev, G.L. Kuryshv, A.S. Larshin, V.G. Polovinkin, *Prikl. Fiz.* 2 (2005) 97–101.
- [20] P.N. Brunkov, N.D. Il'inskaya, S.A. Karandashev, A.A. Lavrov, B.A. Matveev, M.A. Remennyi, N.M. Stus', A.A. Usikova, P-InAsSbP/n-InAs single heterostructure back-side illuminated 8 × 8 photodiode array, *Infrared Phys. Technol.* 78 (2016) 249–253, <https://doi.org/10.1016/j.infrared.2016.08.013>.
- [21] N.D. Il'inskaya, S.A. Karandashev, A.A. Lavrov, B.A. Matveev, M.A. Remennyi, N.M. Stus', A.A. Usikova, InAsSbP photodiodes for the 2.6–2.8 μm wavelengths, *Tech. Phys.* 88 (2) (2018) (in press).